applied sciences

MDPI

Review

Nonlinear Silicon Photonic Signal Processing Devices for Future Optical Networks

Cosimo Lacava *, Mohamed A. Ettabib and Periklis Petropoulos

Optoelectronics Research Centre, University of Southampton, Southampton SO17 1BJ, UK;
mae206@orc.soton.ac.uk (M.A.E.); pp@orc.soton.ac.uk (P.P.)
* Correspondence: C.Lacava@soton.ac.uk; Tel.: +44-23-8059-3186

Academic Editor: Paolo Minzioni
Received: 11 November 2016; Accepted: 25 December 2016; Published: 20 January 2017

Abstract: In this paper, we present a review on silicon-based nonlinear devices for all optical nonlinear processing of complex telecommunication signals. We discuss some recent developments achieved by our research group, through extensive collaborations with academic partners across Europe, on optical signal processing using silicon-germanium and amorphous silicon based waveguides as well as novel materials such as silicon rich silicon nitride and tantalum pentoxide. We review the performance of four wave mixing wavelength conversion applied on complex signals such as Differential Phase Shift Keying (DPSK), Quadrature Phase Shift Keying (QPSK), 16-Quadrature Amplitude Modulation (QAM) and 64-QAM that dramatically enhance the telecom signal spectral efficiency, paving the way to next generation terabit all-optical networks.

Keywords: silicon photonics; nonlinear optics; advanced modulation format; wavelength conversion

1. Introduction

Over the last decade, silicon photonics has established itself as a mature technology for the fabrication of low cost, scalable, optical integrated circuits that can meet the requirements of future optical networks [1]. Silicon-on-Insulator (SOI) is widely acknowledged as the ideal fabrication platform for silicon photonic components, providing a Complementary Metal Oxide Semiconductor (CMOS)-compatible, high-index contrast system. At present, most fundamental signal processing functionalities on optical networks are still performed in the electrical domain, imposing successive optical-to-electrical-to-optical conversions across the network, thereby increasing the system complexity and cost and restricting the maximum bandwidth of the transmitted signals [2]. Nonlinear optical devices have already shown great potential for either substituting or complementing electronic processing for the implementation of certain signal processing functionalities, showing no practical limitations in terms of bandwidth [3]. Thanks to their high refractive index difference (>2) and the strong third-order nonlinear response of silicon [4,5], SOI waveguides have been widely used to observe nonlinear optical effects. SOI devices have substantially contributed to the realization of efficient all optical nonlinear components; a number of fundamental functionalities have been demonstrated in the SOI nonlinear platform such as all optical wavelength conversion [6–9], optical switching [10,11], format conversion [12,13], logic operation [14] and high speed all optical modulation [10,15,16].

However, the large nonlinear response in silicon is also accompanied by strong two-photon absorption (TPA) that causes accumulation of free carriers that induce a very high nonlinear loss [3]. This effect reduces the optical power that can be beneficially coupled into the waveguide, and subsequently the achievable nonlinear phase shift is restricted to fractions of $\pi/2$ radians [3], practically limiting the use of the technology in telecom settings.

Advanced modulation formats, such as multiple (M)-order QAM (Quadrature Amplitude Modulation), have become key to the design of modern high-capacity optical transport networks [17].

Integrated optical components that can operate on these modulation formats are required to enable bandwidth efficient, high speed transmission on a chip level, providing fundamental optical functionalities such as wavelength routing, wavelength conversion, format conversion, etc. Such functionalities have already been demonstrated in silicon-based nonlinear devices in recent years [13,18,19]. However, the devices featured in these works are typically limited by TPA-triggered processes, therefore they suffer from reduced efficiency that makes them unsuitable for practical applications. In order to overcome this limitation, alternative materials have been proposed by the scientific community as AlGaAs [20,21], chalcogenides [22,23], composite glasses [24] and nonlinear polymers [25]. Even though these materials have shown promise for achieving remarkable performance, fabrication constraints make their integration with the standard silicon platform difficult, requiring additional manufacturing steps, which are not desirable in high integration optical platforms. We have recently investigated two material platforms that can be easily integrated with existing silicon photonic infrastructures, namely amorphous silicon and silicon germanium. We have demonstrated wavelength conversion of complex modulation format signals [26–28], phase sensitive regeneration in integrated devices [29,30] and supercontinuum generation in cm-long waveguides [31]. In this paper, we provide a comprehensive review of the latest results on the development of silicon-based nonlinear optical devices for all optical processing of complex modulation formats achieved by our research group through extensive collaborations with various academic partners namely University of Pavia, CEA-Leti, University of Athens and the Technological Educational Institute of Athens. The paper is organized as follows: Section 2 is devoted to the discussion of amorphous silicon based devices, while Section 3 focuses on silicon germanium devices. Section 4 is dedicated to new CMOS compatible materials that are currently being studied in our group and can serve as a platform for future efficient optical nonlinear devices. Finally, conclusions are drawn in Section 5.

2. Amorphous Silicon Waveguides

Amorphous silicon has been identified as possible solution to overcome the main limitations showed by the SOI platform namely TPA and Free Carrier Absorption (FCA) effects [28,32–34] already discussed in the previous section. Indeed, amorphous silicon shows enhanced nonlinear performance with respect to crystalline silicon, exhibiting both an enhanced Kerr response [28,35–37] and a reduced TPA effect [28,38]. Thanks to these properties, a-Si could be used as nonlinear media at higher power levels with respect to silicon, allowing to achieve a π phase shift, even in cm-long waveguide structures. However, material stability issues have been reported [38], which compromise the use of this compound as a nonlinear platform for optical communications. We have recently showed that CMOS compatible hydrogenated amorphous silicon waveguides can be utilized at both low and high power level regimes, showing remarkable performance and stable operation [26,28]. Nonlinear waveguides were fabricated and used to demonstrate low power all optical processing of phase encoded signals, such as DPSK (Differential Phase Shift Keying) and QPSK (Quadrature Phase Shift Keying) [26]. In the following sections, we briefly report the optical characteristics of the developed amorphous silicon waveguides, and show the high speed wavelength conversion experiments using phase-encoded signals.

2.1. Linear and Nonlinear Optical Characterization

Nonlinear waveguides were fabricated at CEA-Leti laboratories on standard thermal oxide 200 mm wafers and their nonlinear properties were demonstrated in [28] for the first time. The thickness and width of the waveguides were set to 220 nm and 480 nm respectively. The sample under test was fabricated starting from a 1.7 µm thick SiO_2 layer. The a-Si layer was deposited by means of the Plasma Enhanced Chemical Vapour Deposition (PECVD) technique at a temperature of 350 °C. A first etching step was used to define grating coupler patterns with an etching depth of 70 nm. The couplers were designed in such a way to only couple the transverse electric mode (TE-mode). After deposition of a silica hard mask, a full etch step (etching depth of 220 nm) was performed to define the waveguide layout. Several straight and serpentine waveguides (with a fixed

480 × 220 nm cross-section) were obtained with lengths varying from 1 mm to 82.6 mm. Finally, a protective 500 nm oxide upper cladding was deposited on the top of the waveguides. A schematic of the waveguide cross-section is shown in Figure 1. Details of the fabrication process can be found in [26,28].

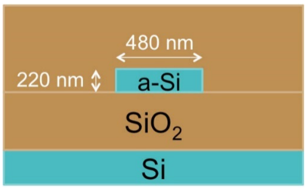

Figure 1. Amorphous silicon waveguide cross section. The thickness of the SiO_2 layer is 1.7 μm [28].

The Kerr response of the a-Si waveguides were evaluated by means of continuous wave (CW) degenerate Four Wave Mixing (FWM) experiments, performed in the C-band wavelength region using waveguides of various lengths as shown in details in [28]. A CW pump beam and a weaker CW signal were combined together and sent to the waveguide under test using a vertical coupling scheme [39]. A typical recorded spectrum, after propagation along the structure under test, is shown in Figure 2 (inset).

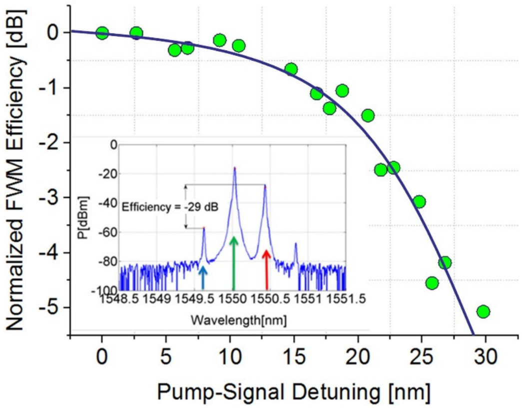

Figure 2. Normalized FWM (Four Wave Mixing) efficiency as a function of pump-signal detuning. The waveguide length was 2.26 cm. Inset: Spectrum recorded after propagation along the waveguide [26,28].

The Re{γ} can be extracted by the measured FWM traces by using the following equation [40]:

$$\mathrm{Re}\{\gamma\} = \frac{\sqrt{P_i(L)/P_s(L)}}{\eta P_p(0) L_{\mathrm{eff}}} \quad (1)$$

where L_{eff} is the effective nonlinear waveguide length, and η accounts for the phase-mismatch induced by waveguide dispersion. By considering spectra obtained from waveguides of different lengths, measured at various pump power levels, a Re{γ} equal to 800 ± 50 $(\mathrm{Wm})^{-1}$ was obtained, which is three times larger with respect to values commonly measured in channel crystalline silicon (c-Si) waveguides [41]. The waveguide dispersion was also evaluated by measuring the FWM efficiency while increasing the pump-signal detuning, as reported in Figure 2. By fitting the curve, a dispersion coefficient D = −380 ps/(nm·km) was obtained.

TPA and Free Carrier Absorption (FCA) coefficients were determined by means of pulsed experiments, as described in detail in [28]. TPA and FCA effects occur when the optical power inside the waveguide is higher than the TPA-threshold, thus triggering the multiple photon absorption and FC-related effects. As the dynamic of TPA is fast (~fs) while FC-effects are typically slower (~ps), their contributions to the overall device absorption can be discriminated by using pulsed and CW experiments [6]. The Im{γ} coefficient was assessed through the use of ultra-short pulses (120 fs pulse duration at 82.5 MHz repetition rate) and its value calculated starting from the following differential equation, where $P(z)$ is the pump power and α_0 is the linear loss [42].

$$\frac{d}{dz}P(z) = -a_0 P(z) - 2|\mathrm{Im}(\gamma)|P^2(z) \tag{2}$$

by assuming a hyperbolic-secant pulse temporal-profile, it is possible to derive analytically the dependence of the average transmitted power, P_T, on the input pulse peak power P_0.

$$P_T = e^{-\alpha_0 L}\frac{\ln\left(\sqrt{2|\mathrm{Im}(\gamma)|L_{\mathrm{eff}}P_0} + \sqrt{1+2|\mathrm{Im}(\gamma)|L_{\mathrm{eff}}P_0}\right)}{\sqrt{(2|\mathrm{Im}(\gamma)|L_{\mathrm{eff}}P_0)(1+2|\mathrm{Im}(\gamma)|L_{\mathrm{eff}}P_0)}}P_0 \tag{3}$$

using the waveguide loss α_0 (estimated to be 4.7 dB/cm) and the pulse peak power that can be extracted from the experimental data, Im{γ} was evaluated by fitting the experimental curve, yielding a value of 15.5 ± 2 $(\mathrm{Wm})^{-1}$. In order to compare the performance of a-Si waveguides to other nonlinear material systems, it is useful to employ a figure of merit (FOM) that accounts both for the Kerr response and the nonlinear losses. This is achieved by the following FOM [42]:

$$\mathrm{FOM} = \frac{1}{4\pi}\frac{\mathrm{Re}\{\gamma\}}{\mathrm{Im}\{\gamma\}} \tag{4}$$

which yields a value of 4.7 for the a-Si waveguides used in this study. This is one order of magnitude higher than typical values quoted for c-Si nonlinear waveguides [3].

The FCA coefficient (α_{FC}) and the carrier dynamics were assessed by performing two different experiments as described in details in [28]. The pulse propagation in the presence of TPA can be described by the following equation [42]:

$$\frac{d}{dz}I(z,t) = -[\alpha_0 + \alpha_{FC}N_{FC}(t)]I(z,t) - \beta I^2(z,t) \tag{5}$$

where N_{FC} is the number of free carriers per unit volume and β the TPA coefficient.

The first experiment, aimed at the evaluation of free carrier recombination time, employed a pump-probe scheme as described in [28]. Results of this experiment are reported in Figure 3 (left panel). It can be noted that when the peak power of the pump pulses was relatively low (P_0 < 10 dBm in the waveguide), the transmission power of the probe was almost constant in time, while for P_0 > 10 dBm depletion of the probe beam was observed in the present of a pump pulse.

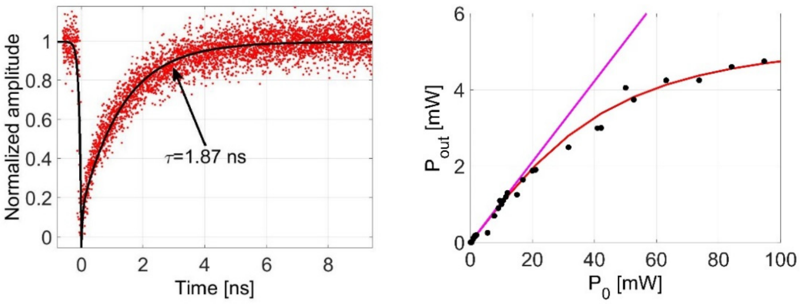

Figure 3. (**Left**) Free carrier recovering time experimental trace (P_0 = 10 W); and (**Right**) example of the transmission curve used to estimate α_{FC} (L = 2.26 cm); black circles are the experimental data, the red trace is the fitting function and the purple line represents the theoretical curve without TPA (two-photon absorption) and FCA (Free Carrier Absorption) effects [28].

This can be attributed to the abrupt rise of N_{FC} induced by TPA and can be described through the following equation:

$$\frac{d}{dt}N_{FC}(z,t) = \frac{\beta I^2(z,t)}{2h\omega_0} - \frac{N_{FC}(z,t)}{\tau} \tag{6}$$

after the initial power drop, caused by the TPA-excited free-carriers, a two-phase recovery process can be observed: a very fast process responsible for the initial recovery of about 10% of transmission, and a second (slower) process yielding a relatively long power-recovery tail. Experimental data can be fitted by the superposition of two exponential functions with time constants $\tau_1 < 50$ ps (fast recovery) and $\tau_2 = 1.87$ ns.

In order to evaluate the additional loss induced by free carriers, a second experiment was carried out using a single CW beam. In this case, the beam intensity evolution along the waveguide can be written as [42]:

$$\frac{d}{dz}I(z) = -\alpha_0 I(z) - \beta I^2(z) - \alpha_{FC}\frac{\beta\tau}{2h\omega_0}I^3(z) \tag{7}$$

α_0, β and τ parameters were previously determined. The value of α_{FC} can then be determined by experimentally measuring the transmission curve of a waveguide and fitting the data to Equation (7). This is shown in Figure 3 (right), which indicates a value $\alpha_{FC} = 0.8 \times 10^{-17}$ cm^2. This is only slightly lower than that measured in c-Si waveguides ($\alpha_{FC} = 1.1 \times 10^{-17}$ cm^2) [42].

The overall optical characteristics of the amorphous silicon waveguides are outlined in Table 1.

Table 1. a-Si waveguide optical characteristics determined in [28].

α_0 (dB/cm)	Re{γ} (Wm)$^{-1}$	Im{γ} (Wm)$^{-1}$	Free Carrier (FC) Recovery Time (ns)	α_{FC} (cm^2)
4.7	800 ± 50	15.5 ± 2	1.87	0.8×10^{-17}

a-Si has been studied by numerous research groups in the last ten years. Remarkable results have been demonstrated in terms of nonlinear optical properties [32,38,43,44] which are in accordance to what we report in this manuscript. However, the a-Si material microstructure is strongly affected by the layer deposition parameters used during the fabrication steps, therefore different performing a-Si alloys can be found in the literature. In Table 2, we show some recent results that have been reported, mainly in terms of Kerr and TPA response.

Table 2. a-Si materials reported in the literature.

Reference	Re{γ} (Wm)$^{-1}$	Im{γ} (Wm)$^{-1}$	FOM (Figure Of Merit)
[26]	800	15	4.7
[35]	332	5.43	4.9
[32]	1200	12.5	7.6
[36]	770	19.6	3.12
[45]	2003	205	0.85

2.2. All Optical Wavelength Conversion of DPSK and QPSK Signals

Benefitting from the nonlinear properties of the a-Si waveguides described is the previous section, wavelength conversion experiments at 20 Gb/s using either BPSK or QPSK signals were performed. The experimental set-up used for these experiments was first reported in [26] and is shown in Figure 4. One-millimeter-long waveguides were used for these experiments. The power of the CW pump inside the a-Si waveguide (estimated after taking into account the grating coupler losses) was set to 70 mW, well below the TPA threshold of the waveguide. An optical spectrum recorded at the waveguide output when a BPSK (Binary Phase Shift Keying) signals was used at its input is shown in Figure 5a. The measured FWM conversion efficiency was measured to be −26 dB. Constellation diagrams for both the original BSPK signal (back to back configuration) and DPSK idler are also shown in the figure. Figure 5b shows Bit Error Rate (BER) curves measured for the back-to-back (B2B) and the converted signal revealing that successful wavelength conversion was obtained with only 1 dB of power penalty at a BER = 10^{-5}.

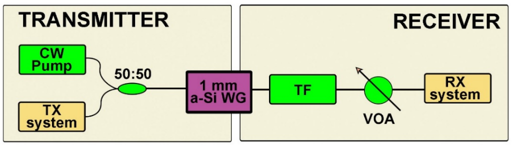

Figure 4. Wavelength conversion experiment set-up. TF: Tunable filter. CW: Continuous Wave; TX: Transmitter [26].

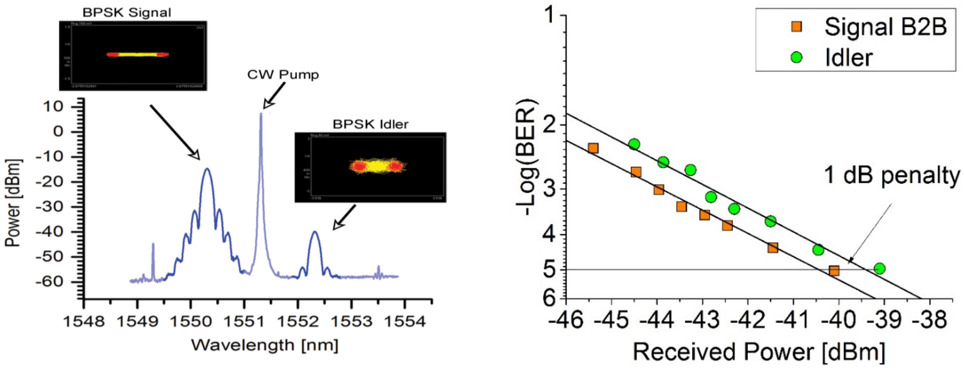

(a) (b)

Figure 5. (**a**) Output DPSK (Differential Phase Shift Keying) spectra (resolution 0.05 nm) recorded at the waveguide output. Signal and Idler constellation diagrams are also shown as insets; (**b**) BER (Bit Error Rate) measurements for a 20 Gb/s BPSK signal. Input pump power was set to 70 mW [26].

Wavelength conversion experiments using QPSK signals were also carried out. The input signal was a 10 Gbaud QPSK signal carrying a 20 Gb/s pseudorandom data sequence. Results obtained with this signal are outlined in Figure 6.

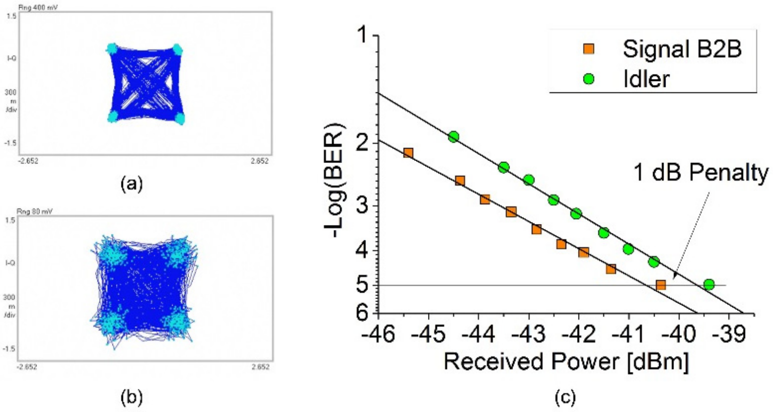

Figure 6. (**a**) QPSK (Quadrature Phase Shift Keying) B2B (back-to-back) and (**b**) converted constellation diagrams; (**c**) BER results [26].

Figure 6a,b shows constellation diagrams for both the B2B and the converted signal, whereas Figure 6c shows a comparison of the BER values obtained for these two signals. A penalty of 1 dB is observed at a BER = 10^{-5} demonstrating that the waveguide can be used for the processing of fast, complex-modulation optical signals.

In this section, we showed the optical characteristics of the hydrogenated amorphous silicon platform [28] and briefly reviewed the performance of fabricated waveguides when used as all-optical wavelength converters for phase-encoded telecommunication signals [26]. Thanks to the absence of TPA in the C-band wavelength region, these devices can be considered as building blocks for applications in future all-optical networks. It is also worth noting that similar results, in terms of conversion efficiency and Optical Signal to Noise Ratio (OSNR) penalty, have been achieved in other platforms, such as crystalline silicon [18,46], AlGaAs on SOI [47] or in semiconductor optical amplifiers (SOA)-based devices [48]. Please refer to Table 5 for a more detailed comparison between other nonlinear platforms and the a-Si pretended in here.

3. Silicon Germanium Waveguides and Nonlinear Applications

Silicon germanium has emerged as an attractive platform for implementing both micro- and opto-electronic devices thanks to the potential it offers for bandgap and lattice parameter engineering [49]. Multiple SiGe device demonstrations have already been reported such as modulators [50], light emitters [51] and photodetectors [52,53]. Furthermore, SiGe also offers the potential for implementing efficient nonlinear applications in the midwave and longwave infrared due to the stronger nonlinearities it possessed as compared to pure Si [31,54].

Until recently, the absorptive properties of Ge at the near-infrared region have restricted the applicability of the SiGe platform at this wavelength regime to mostly detection applications. However, it has been recently demonstrated that through an appropriate design one can engineer SiGe devices that exhibit excellent optical properties for nonlinear applications at telecommunication wavelengths [55]. The percentage of Ge concentration is found to impact a host of optical characteristics of the SiGe device, such as linear and nonlinear loss, nonlinearity, dispersion and modal properties. As such, the SiGe platform offers a unique versatility and a strong potential for realizing a wide range of efficient all-optical signal processing applications at the near-infrared, particularly those that require strict phase matching conditions.

In this section, we review the main optical properties of the $Si_{1-x}Ge_x$ alloy as well as the results of wavelength conversion of 16-QAM and 64-QAM signals.

3.1. Linear and Nonlinear Optical Characterization

Below we summarize the optical properties of SiGe waveguides for different Ge concentrations and waveguide widths at telecommunication wavelengths (λ = 1530–1580 nm). The impact of these two parameters on the linear and nonlinear loss and Kerr nonlinearity were studied and presented in detail in [55]. The waveguides studied were strip-waveguides encapsulated in a 12 µm top silicon cladding layer and fabricated by means of the Reduce Pressure Chemical Vapour Deposition (RP-CVD) technique.

3.1.1. Linear Loss

SiGe waveguides with a fixed waveguide height of 1.4 µm and widths varying between 0.3–2 µm and Ge concentrations between 10%–30% were characterized in terms of linear loss using the Fabry–Pérot (FP) resonances technique [56]. Table 3 presents a summary of the measurement results. For a fixed waveguide width, the increase in Ge concentration strongly increases the absorption loss. However, it is noted that waveguides with low Ge concentration (x = 0.1) and small widths (≤1.0 µm) also exhibit very high losses. This is due to the small confinement factors of these waveguides, which justifies the high loss figures reported. A full discussion of the loss trends along with a numerical analysis of the confinement factors and effective mode areas of the waveguides studied is presented in [55].

Table 3. Linear loss figures for $Si_{1-x}Ge_x$ waveguides with varying widths and Ge concentration (x) [55].

Ge Concentration/ Waveguide Width	0.3 µm	0.6 µm	0.8 µm	1 µm	1.5 µm	2 µm
x = 0.1	High loss (> 5 dB/cm)			4.75 dB/cm	0.43 dB/cm	0.65 dB/cm
x = 0.2	3.90 dB/cm	2.38 dB/cm	2.38 dB/cm	1.40 dB/cm	1.52 dB/cm	2.60 dB/cm
x = 0.3	3.47 dB/cm	4.56 dB/cm	4.77 dB/cm	5.21 dB/cm	4.77 dB/cm	4.34 dB/cm

3.1.2. Kerr Nonlinearity

The same group of waveguides was characterized in terms of nonlinearity using the CW-FWM method [42]. The results are summarized in Figure 7. As expected, the nonlinearity (Re{γ}) increases with Ge concentrations (because of the increased optical mode confinement, i.e., reduced A_{eff}). Furthermore, waveguides with smaller width exhibit larger values of Re{γ} up to a width (typically between 0.6 µm and 0.8 µm) where the mode can no longer be confined in the waveguide and the trend is reversed. The figure also shows a good agreement between the experimental measurements of Re{γ} and those predicted by simulations [55].

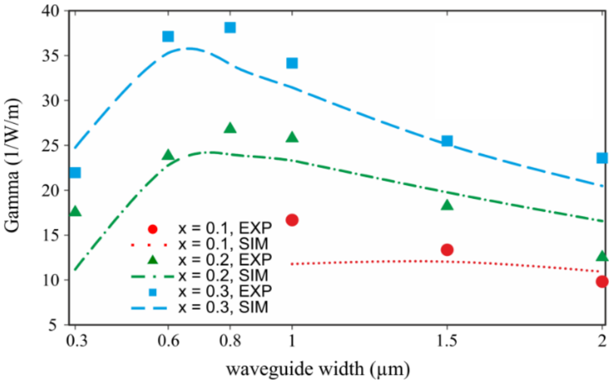

Figure 7. A comparison of experimental and numerical results of the nonlinear coefficient measurement as a function of the waveguide width for varying Ge concentration [55].

3.1.3. Two-Photon Absorption

A TPA coefficient measurement for a waveguide of width of 2 µm and varying Ge concentration was carried out using the inverse transmission method [25], as shown for the first time in [55]. Figure 8 shows the inverse transmission (ratio of input to output power) as a function of the input peak power for the three different Ge concentrations and for a waveguide width of 2 µm. A clear increase in TPA is observed when the Ge concentration increases. By adopting a linear fit to these measurements [6], the TPA coefficient values were found to be 1.16 cm/GW, 1.24 cm/GW and 1.5 cm/GW for an increasing Ge concentration from 10% to 30%. A comparative theoretical and experimental discussion of TPA properties in SiGe waveguides is presented in detail in [55]. By combining the obtained values for both the Re{γ} (Section 3.1.2) and Im{γ} (this section) it is possible to calculate the FOM (as defined in Equation (4)) for the three different Ge concentrations, obtaining 0.53, 0.43 and 0.58 for Ge concentration of 10%, 20% and 30%, respectively. Even though they are not as high as in the case of amorphous silicon, these values are slightly higher than what reported for crystalline silicon waveguides [3].

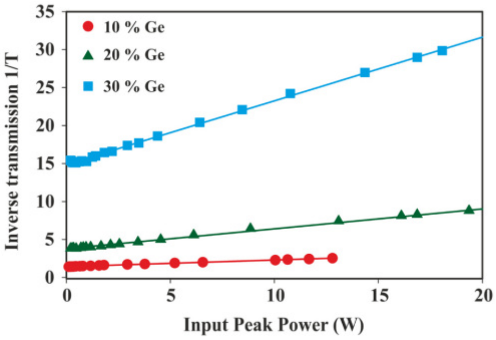

Figure 8. A plot of the inverse transmission vs. coupled input peak power measurement for a waveguide of 2 µm width and varying Ge concentrations [55].

Re{γ}, Im{γ} and FOM values are reported in the following Table 4 for three selected SiGe waveguide configurations [55].

Table 4. Nonlinear parameters for three selected SiGe waveguides.

	Re{γ} (Wm)$^{-1}$	**Im{γ} (Wm)$^{-1}$**	**FOM**
W = 1000 nm, Ge (10%)	16	0.76	1.67
W = 1000 nm, Ge (20%)	25	1.16	1.71
W = 1000 nm, Ge (30%)	35	1.98	1.40

3.2. Wavelength Conversion of 16-QAM and 64-QAM Signals:

The performance of SiGe waveguides as nonlinear processors for telecommunication signals was tested in wavelength conversion experiments. These demonstrations (detailed in [57]) used 10 Gbaud 16- and 64-QAM signals and were conducted in the 1550 nm wavelength region. The SiGe device used featured a strip air-clad structure with a 0.6 µm width and a 1.6 µm height and whose fabrication process was similar to that described in [31,55].

The experimental setup used for the wavelength converter is similar to that implemented for the DSPK and QPSK wavelength conversion in the amorphous silicon waveguide (Section 2.2, Figure 4). Figure 9a depicts a typical optical spectrum obtained at the output of the waveguide after converting a 10-Gbaud 16-QAM signal. As can be seen, an idler with a large OSNR exceeding 36-dB was generated with a conversion efficiency of −9.7 dB. Furthermore, a uniform FWM CE exhibiting less than 0.5 dB variation was observed in the signal detuning range between 1548.39 nm and 1564 nm (Figure 9b).

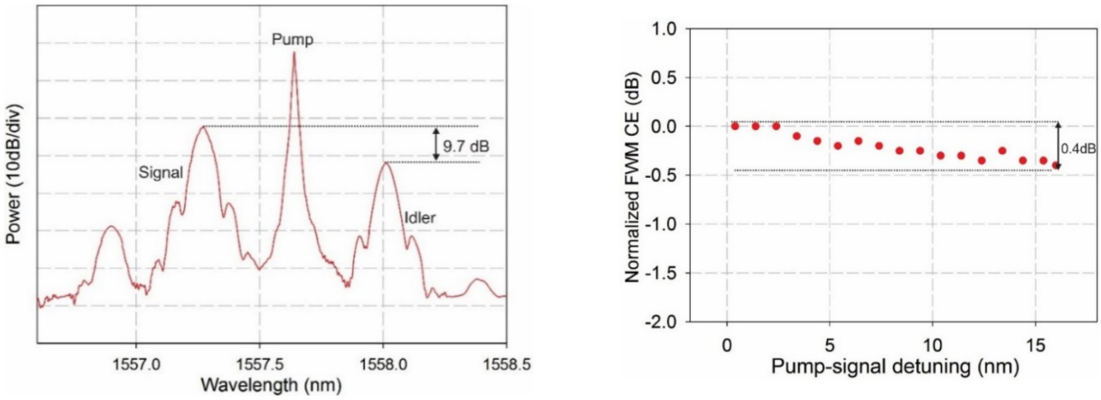

(**a**) (**b**)

Figure 9. (**a**) Output optical spectrum of the wavelength converter; and (**b**) normalized FWM conversion efficiency (dB) as a function of pump-signal detuning (nm).

Figure 10a shows the constellation diagrams and BER curves assessed before and after the wavelength conversion process for both the 16-QAM (Figure 10a) and 64-QAM signals (Figure 10b). The 16-QAM measurements showed an almost identical rms error vector magnitude (EVM) between the B2B signal (8.6%) and the idler (8.7%). Furthermore, a negligible BER penalty of less than 0.3 dB at a BER of 10^{-3} was obtained.

For the 64-QAM case, a similar performance level was achieved. The rms EVM figures of both the B2B and the idler were similar, with 15.5% measured for the B2B and 15.8% for the idler. Furthermore, the two BER curves are similar with an error floor developing on the converted signal at high values of received power (note that the BER of the 64-QAM signal (5.9×10^{-2}) was limited by the bandwidth (9.6 GHz at −20 dB) and effective number of bits of our Arbitrary Waveform Generator (AWG). Both sets of results in Figure 10 demonstrate that the wavelength converter results in almost no loss in quality in the converted signal (idler) in comparison to the original B2B signal and highlight the potential of the SiGe platform in implementing a wide range of state-of-art all-optical signal processing applications.

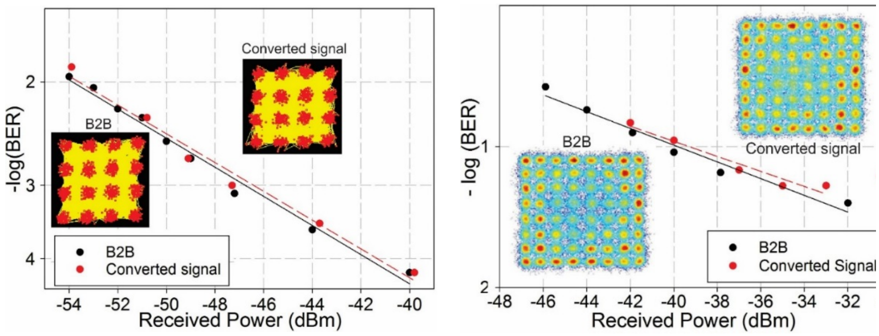

(**a**) (**b**)

Figure 10. BER curves and constellation diagrams for the: 16-QAM (Quadrature Amplitude Modulation) (**a**); and 64-QAM (**b**), before and after the wavelength conversion process.

In Table 5, we compare both a-Si and SiGe wavelength converters and their key performance against other similar devices already presented in the literature, showing conversion of complex, phase encoded telecom signals:

Table 5. Integrated wavelength converter technology comparison.

Device	Signal Type	Conversion Efficiency (dB)	3 dB Conversion Bandwidth (nm)	OSNR [1] Penalty	CMOS [1] Compatible
a-Si (this work reported in [26])	10 Gbaud DPSK [1]	−26 dB	~25 nm	<1 dB	Yes
Si-Ge (this work reported in [57])	10 Gbaud 64 QAM [1]	−9.7 dB	~30 nm	<1 dB	Yes
c-Si [18]	28 Gbaud 16 QAM	−17.5 dB	~30 nm	4 dB at BER [1] = 10^{-5}	Yes
AlGaAs on SOI [47]	10 Gbaud 256 QAM	−13 dB	~28 nm	2.5 dB	No
Hydex [58]	10 Gbaud 16 QAM	−40 dB	~10 nm	0.5 dB	Yes

[1] OSNR: Optical Signal to Noise Ratio; CMOS: Complementary Metal Oxide Semiconductor; DPSK: Differential Phase Shift Keying; QAM: Quadrature Amplitude Modulation; BER: Bit Error Rate.

Crystalline silicon has been widely used to realize all optical wavelength converters as shown for example in [7,46]. In Table 5, we only report the most advanced result (in terms of signal complexity), showing the wavelength conversion of a 112 Gb/s 16 QAM signal. Although the efficiency of these devices can be improved, we believe that their main limitation is represented by the combination of TPA and FC's effects, which limit the maximum pump power that can be injected in the waveguide, thus reducing the achievable conversion efficiency. A biased waveguide can be used to mitigate the impact of FCA as shown in [19], however this approach requires additional fabrication steps that might be not desirable. Impressive results have been recently shown by using AlGaAs waveguides [47], however this platform is not CMOS compatible and may require high temperature fabrication steps [20,21] to reduce the propagation losses. Hydex offers both relatively high nonlinearity and extremely low loss at the telecom wavelength region [24], however very long waveguides are typically required to obtain the desired conversion efficiency (of the order of meters). Both a-Si and SiGe platforms offer remarkable nonlinear performance as shown in this manuscript, also offering the additional flexibility to tune the linear and nonlinear optical properties of the platform by changing the material deposition parameters. We believe that the two proposed platforms (a-Si and SiGe) are now sufficiently mature, facilitating the realization of reliable and efficient devices for the future all optical settings.

3.3. Low Birefringence SiGe Waveguides

The impact of Ge concentration on a host of optical properties means an additional flexibility in creating nonlinear photonic devices with specific phase matching and/or modal characteristics. One specific example that this versatility facilitates is the ease of realizing low-birefringence nonlinear waveguides.

Low birefringence behavior, characterized by the presence of a significant Transverse Electric (TE)/Transverse Magnetic (TM) modal symmetry, is a crucial requirement in many signal processing applications that utilize vector parametric processes such as polarization-insensitive wavelength conversion. It was shown, that a strong TE/TM mode similarity across a broad wavelength range as well as a large nonlinear coefficient can be achieved in SiGe devices through multiple device designs and structural geometries [27,30,54,55]. In particular, it was found that a buried device structure (i.e., encapsulating the waveguide in a Si layer) allows a simple and effective route towards combining low loss, high nonlinearity and low birefringence behavior.

Figure 11 shows the calculated dispersion curves as well as the nonlinear coefficient of the two polarization axes of a 1 μm $Si_{0.8}Ge_{0.2}$ buried waveguide around the 1.55 μm region where the two polarization modes were predicted to exhibit very similar dispersion and nonlinearity across the 1.40–1.70 μm band [30,55]. There properties were exploited to demonstrate the first single-pass polarization-insensitive wavelength converter in a silicon-based device [27], achieving a polarization dependent loss (PDL) of 0.42 dB only. Furthermore, these SiGe devices were utilized to demonstrate the first passive and CW-pumped polarization-assisted (PA) phase sensitive amplifier (PSA) in a silicon-based waveguide exhibiting a record phase sensitive extinction ratio (PSER) of 28.6 dB for a low input pump power [29,30]. These demonstrations highlight the versatility of the SiGe platform and its emergence as a competitive technology and a promising candidate for a wide range of all-optical signal processing applications. Please refer to Ref. [27] for a more detailed description of the device shown in Figure 11 and the capabilities of such designed devices.

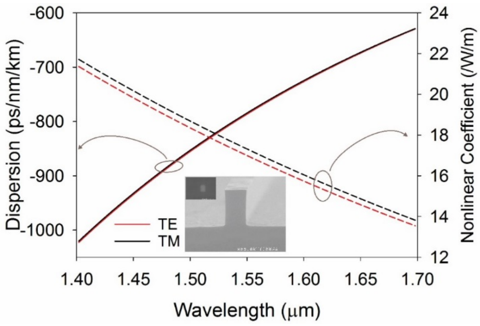

Figure 11. Dispersion and nonlinear coefficient curves for the structure under investigation as a function of wavelength. Inset: Scanning Electron Microscope (SEM) image of the 1 μm wide SiGe strip waveguide before and after encapsulation in a 12 μm Si cladding layer [27].

4. Novel Materials for All Optical Processing Nonlinear Devices

In this section, we review some alternative materials that have emerged recently as promising candidates for the implementation of nonlinear processing devices.

4.1. Engineered Silicon Rich Silicon Nitride

Silicon nitride has become a material of great interest in the field of nonlinear optics in recent years [59–62]. A variety of nonlinear applications have already been demonstrated, such as wavelength conversion [60], supercontinuum generation [59] and harmonic generation [63]. Silicon nitride is a CMOS compatible composite that can be deposited on a SiO_2 layer, providing a suitable alternative to c-Si. Thanks to its optical properties, by carefully controlling the material fabrication conditions, very low loss waveguides can be obtained. Furthermore, no TPA is observed in the C-band wavelength region, making this platform suitable for both low and high power applications. However, the use of this platform as a nonlinear tool is still hindered by fabrication difficulties that prevent the possibility of growing thick SiN layers on SiO_2 (>200 nm) [24], thus drastically reducing the ability of confine light tightly within the core material, and in turn limiting the overall nonlinear response of the device. Moreover, the silicon nitride Kerr coefficient is substantially lower than that in silicon [64] (two orders of magnitude lower), further reducing the strength of the nonlinear effects. Recently, a number of research groups have proposed the use of silicon-enriched silicon nitride compounds, aiming to increase the device nonlinear response [59,65–68]. This direction, however, introduces additional losses in the waveguides [66,68], that may compromise their suitability for practical applications. We have recently studied systematically the impact of introducing silicon within a silicon nitride matrix using only CMOS Back End Of Line (BEOL) fabrication processes, on both linear and nonlinear optical properties [68,69]. We outline here the most important outcomes of this study, demonstrating that by carefully selecting the fabrication conditions a TPA free, low loss, highly nonlinear waveguide configuration can be obtained, overcoming most of the issues imposed by the introduction of silicon when designing a nonlinear device.

In order to evaluate the effect of enriching silicon nitride with silicon, three different material compositions were developed and deposited on thermal SiO_2 wafers. The wafer composition is schematically shown in Figure 12.

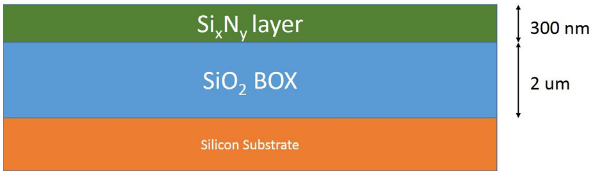

Figure 12. Schematic representation of wafer compositions.

The resulting refractive indices of the three fabricated wafers (identified as Wafer_01, Wafer_02 and Wafer_03 hereafter) are shown in Table 6. Various test structures (including straight waveguides of different lengths and widths) were defined onto the wafers by using a standard dry etch technique. In order to evaluate the linear and nonlinear properties of the fabricated waveguides as a function of the introduced silicon excess, three different parameters were considered: (1) waveguide linear loss α_0; (2) Kerr response coefficient Re{γ}; and (3) TPA coefficient Im{γ}, all evaluated across the whole C-band wavelength region. The waveguide linear losses were evaluated by using a standard cutback technique. The optical transmission of waveguides of varying lengths was evaluated, providing the α_0 coefficient for each width configuration. Re{γ} and Im{γ} were both evaluated utilizing techniques shown in Section 2, by using CW-FWM and pulsed transmission experiments, respectively. The obtained results for a representative waveguide (Width = 1000 nm, Height = 300 nm) are shown in Table 6.

Table 6. Extracted optical characteristics for different silicon-rich silicon nitride material compositions.

	Material Refractive Index	α_0 (dB/cm)	Re{γ} $(Wm)^{-1}$	Im{γ} $(Wm)^{-1}$
Wafer_01	2.01	1.38	1.54	Negligible
Wafer_02	2.49	1.5	16	Negligible
Wafer_03	2.79	5.5	28	2.58

It is clear from Table 6 that higher linear losses were observed when the silicon content contained in the compound was increased; it is noted however, a modest increase was observed in Wafer_02, while a significantly higher value was measured for Wafer_03. On the other hand, like Wafer_01, the composition of which is very close to stoichiometric Si_3N_4, Wafer_02 still did not show any

TPA-related effects, exhibiting an enhanced Kerr response at the same time. By combining this information, we can conclude that there are material compositions that offer a good trade-off between linear loss and nonlinear response, and provide TPA-free waveguides that can be used as nonlinear processor units at communication wavelengths [68,69]. The Kerr response of Wafer_02 waveguides ($\mathrm{Re}\{\gamma\} = 16\ (\mathrm{Wm})^{-1}$) is similar to what previously reported for SiGe waveguides [55], but the lower linear loss (~1.5 dB/cm) and the absence of TPA represent a clear advantage over the SiGe technology, allowing for high power, low loss, nonlinear applications. Both amorphous silicon [28,32] and crystalline silicon [18] show higher Kerr response with respect to our Si rich silicon nitride material (an order of magnitude higher); however TPA and FCA effects are still present and hinder the high power operation on these devices.

4.2. CMOS Compatible Tantalum Pentoxide Waveguides for Nonlinear Optical Processing

Tantalum pentoxide (Ta_2O_5) is a CMOS compatible material that has been studied in the past for its nonlinear applications at 980 nm and has only very recently been considered as a possible alternative for telecom-wavelength applications. Thanks to its extremely large band-gap value (3.8 eV), no TPA effect is present at the 1550 nm wavelength region, making this material an ideal candidate for nonlinear optical processes in waveguides integrated on a SOI substrate [70–72]. Here, we briefly review the nonlinear optical properties of low loss $Yb{:}Ta_2O_5$ rib waveguides integrated on the top of a SiO_2 layer reported for the first time in [71].

Nominally 1 µm thick $Yb{:}Ta_2O_5$ films were deposited by RF magnetron sputter deposition from a powder-pressed Ta_2O_5 target doped with 2.5 wt. % of ytterbium oxide onto a four inch silicon substrate with a 2.5 µm thick thermally-grown silica layer. Waveguides were defined by using standard photolithography and Ion Beam Milling (IBM). Strips of photoresist of widths varying from 1 µm to 10 µm in steps of 0.2 µm were defined in positive photoresist spun onto the deposited $Yb{:}Ta_2O_5$ film. Etching was then performed using an ion beam etch and deposition system. To reduce any stresses and oxygen deficiency introduced during the sputtering and etching processes, the wafer was then annealed for two hours at 600 °C. Additional details on the fabrication process can be found in [70,71,73]. A schematic representation and a SEM image of a fabricated waveguide are shown in Figure 13. Through CW-FWM experiments, the nonlinear parameter $\mathrm{Re}\{\gamma\}$ was evaluated and by using the simulated effective area we extracted the nonlinear refractive index was determined to be equal to $6.65 \times 10^{-18}\ \mathrm{m}^2/\mathrm{W}$, which is of the same order of magnitude as in silicon. Propagation losses of the waveguide were also measured to be 0.19 dB/cm. It is also worth noting that no TPA and FCA effects were observed in the 1550-nm region, even at relatively high power operation (peak power >20 W), suggesting that this material can be operated at both low and high power levels. In order to test the material stability, transmission experiments with a CW light beam (kept at a constant power level of 2.5 W) were carried out revealing no material degradation even after >8 h of continuous light feeding. No damage was observed during these measurements, confirming that Ta_2O_5 can be an ideal alternative for applications requiring high power operation.

Importantly, it has been shown that Ta_2O_5 can be used as a host material for many dopants and can therefore be used as a gain material for laser applications [73]. The implications of this for silicon photonics can be significant, since the integration of Ta_2O_5 on the silicon platform could introduce several functionalities that are vital for the development of fully operational, multifunctional, optical transceivers for next generation optical communications.

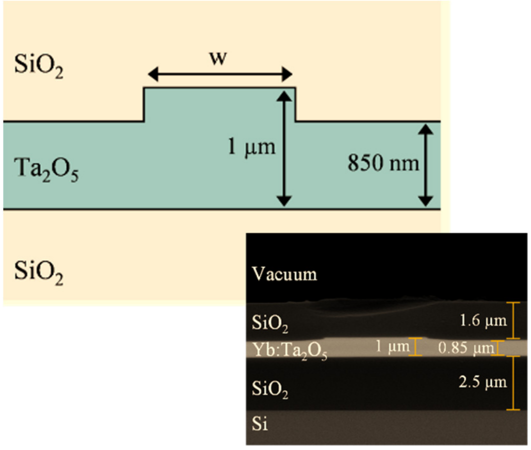

Figure 13. Cross section of the Ta_2O_5 RIB waveguide; and (**inset**) SEM image of the fabricated final device covered by 1.6 μm of SiO_2 (width = 5 μm) [71].

5. Conclusions

In this paper, we have reviewed some recent developments on compact nonlinear devices for all optical signal processing. We have shown results achieved using different integrated optics platforms, and focused mainly on those achieved in amorphous silicon and silicon germanium. We have shown wavelength conversion of complex modulation signals, such as 16-QAM and 64-QAM, demonstrating that both amorphous silicon and silicon germanium platforms are now sufficiently mature to provide a reliable fabrication platform for the development of practical devices for future communication networks based on advanced modulation formats.

Amorphous silicon exhibits a very high nonlinear Kerr parameter ($\mathrm{Re}\{\gamma\}$ ~800 $(\mathrm{Wm})^{-1}$) with a reduced TPA effect with respect to c-Si devices, at telecom wavelengths. On the other hand, linear loss are still relatively high, making this platform not suitable for the realization of long waveguides (>1 cm). The silicon germanium technology offers a unique platform that is suitable for the development of nonlinear devices at both communications and mid-IR wavelengths. Furthermore, the possibility to control the refractive index profile by engineering the Ge concentration in the SiGe alloy allows obtaining a very high refractive index contrast (>2.5) between the waveguide core (SiGe) and the cladding (SiO_2 or air), greatly enhancing the waveguide Kerr response. TPA is also higher in SiGe waveguides with respect to c-Si and a-Si waveguides, however it has been demonstrated that nonlinear optical processing can be performed in these structures by using pump power levels that are still below the TPA-threshold at the communication wavelength region.

In the final section, we have reviewed work towards the development of novel materials that can provide enhanced performance with respect to pure silicon, along with a full CMOS-BEOL compatibility that can facilitate integration with existing silicon photonics components. In this context, silicon-rich silicon nitride and tantalum pentoxide are both seen as promising platforms, showing enhanced nonlinear response along with a complete absence of TPA effects at the telecom wavelength region.

Acknowledgments: The authors would like to acknowledge Ilaria Cristiani and Jean Marc Fedeli for their contributions towards the realization and the study of the amorphous silicon waveguides; Adonis Bogris, Alexandros Kapsalis and Dimitris Syvridis for their contributions on the design and modeling of silicon germanium waveguides; Pierre Labeye, Sergio Nicoletti, and Mickael Brun for the fabrication of the silicon germanium waveguides; and James Wilkinson and Armen Aghajani for the design and fabrication of tantalum pentoxide waveguides. This work was supported by the European Communities Seventh Frame-work Programme FP7/2007-2013 under Grant 288304 (STREP CLARITY) and the Photonics Hyperhighway Programme Grant (EPSRC grant EP/I01196X) and by the Engineering and Physical Sciences Research Council (EPSRC) under the grant "Silicon Photonics for Future Systems" (SPFS) (http://doi.org/10.5258/SOTON/403875).

Author Contributions: C.L. and M.A.E. performed the experimental characterization of the amorphous silicon waveguides. C.L. analyzed the data regarding the amorphous silicon experiments. C.L. and M.A.E. performed the experiments on the SiGe waveguides and consequently analyzed the data. C.L. has developed the Si-rich SiN material described in here. C.L. has performed the experiments on the Ta_2O_5 waveguides and analyzed the extracted data. C.L., M.A.E. and P.P. wrote the paper. P.P. provided the overall supervision and technical leadership. All authors reviewed the manuscript.

Conflicts of Interest: The authors declare no conflict of interest.

References

1. Doerr, C.R. Silicon photonic integration in telecommunications. *Front. Phys.* **2015**, *3*, 1–16. [CrossRef]
2. Jalali, B.; Fathpour, S.; Reed, G.T. Silicon photonics. *IEEE Microw. Mag.* **2006**, *24*, 58–68. [CrossRef]
3. Leuthold, J.; Koos, C.; Freude, W. Nonlinear silicon photonics. *Nat. Photonics* **2010**, *4*, 535–544. [CrossRef]
4. Dinu, M.; Quochi, F.; Garcia, H. Third-order nonlinearities in silicon at telecom wavelengths. *Appl. Phys. Lett.* **2003**, *82*, 2954–2956. [CrossRef]
5. Lin, Q.; Zhang, J.; Piredda, G.; Boyd, R.W.; Fauchet, P.M.; Agrawal, G.P. Dispersion of silicon nonlinearities in the near infrared region. *Appl. Phys. Lett.* **2007**, *91*, 1–4. [CrossRef]
6. Vallaitis, T.; Bogatscher, S.; Alloatti, L.; Dumon, P.; Baets, R.; Scimeca, M.L.; Biaggio, I.; Diederich, F.; Koos, C.; Freude, W.; et al. Optical properties of highly nonlinear silicon-organic hybrid (SOH) waveguide geometries. *Opt. Express* **2009**, *17*, 17357–17368. [CrossRef] [PubMed]
7. Rong, H.; Kuo, Y.-H.Y.; Liu, A.; Paniccia, M.; Cohen, O. High efficiency wavelength conversion of 10 Gb/s data in silicon waveguides. *Opt. Express* **2006**, *14*, 1182–1188. [CrossRef]
8. Lee, B.; Biberman, A. Demonstration of broadband wavelength conversion at 40 Gb/s in silicon waveguides. *Photonics Technol. Lett.* **2009**, *21*, 182–184. [CrossRef]
9. Hu, H.; Ji, H.; Galili, M.; Pu, M.; Peucheret, C.; Christian H Mulvad, H.; Yvind, K.; Hvam, J.M.; Jeppesen, P.; Oxenløwe, L.K. Ultra-high-speed wavelength conversion in a silicon photonic chip. *Opt. Express* **2011**, *19*, 19886–19894. [CrossRef] [PubMed]
10. Lacava, C.; Strain, M.J.; Minzioni, P.; Cristiani, I.; Sorel, M. Integrated nonlinear Mach Zehnder for 40 Gbit/s all-optical switching. *Opt. Express* **2013**, *21*, 21587–21595. [CrossRef] [PubMed]
11. Glesk, I.; Bock, P.J.; Cheben, P.; Schmid, J.H.; Lapointe, J.; Janz, S. All-optical switching using nonlinear subwavelength Mach-Zehnder on silicon. *Opt. Express* **2011**, *19*, 14031–14039. [CrossRef] [PubMed]
12. Astar, W.; Driscoll, J.; Liu, X.; Dadap, J. Conversion of 10 Gb/s NRZ-OOK to RZ-OOK utilizing XPM in a Si nanowire. *Opt. Express* **2009**, *17*, 12987–12999. [CrossRef] [PubMed]
13. Lu, Y.; Liu, F.; Qiu, M.; Su, Y. All-optical format conversions from NRZ to BPSK and QPSK based on nonlinear responses in silicon microring resonators. *Opt. Express* **2007**, *15*, 14275–14282. [CrossRef] [PubMed]
14. Li, F.; Vo, T.D.; Husko, C.; Pelusi, M.; Xu, D.X.; Densmore, A.; Ma, R.; Janz, S.; Eggleton, B.J.; Moss, D.J. All-optical XOR logic gate for 40 Gb/s DPSK signals via FWM in a silicon nanowire. In Proceedings of 24th Annual of the IEEE Photonic Society, Crystal Gateway Marriott, Arlington, VA, USA, 9–13 October 2011; Volume 19, pp. 593–594.
15. Vallaitis, T.; Hillerkuss, D.; Li, J.; Bonk, R.; Lindenmann, N.; Dumon, P.; Baets, R.; Scimeca, M.L.; Biaggio, I.; Diederich, F.; et al. All-Optical Wavelength Conversion Using Cross-Phase Modulation at 42.7 Gbit/s in Silicon-Organic Hybrid (SOH) Waveguides. In Proceedings of PS'09 International Conference on Photonics in Switching, Pisa, Italy, 15–19 September 2009; pp. 2–3.
16. Martínez, A.; Blasco, J.; Sanchis, P.; Galán, J.V.; García-Rupérez, J.; Jordana, E.; Gautier, P.; Lebour, Y.; Hernández, S.; Guider, R.; et al. Ultrafast all-optical switching in a silicon-nanocrystal-based silicon slot waveguide at telecom wavelengths. *Nano Lett.* **2010**, *10*, 1506–1511. [CrossRef] [PubMed]
17. Winzer, P.; Essiambre, R. Advanced Modulation Formats for High Capacity Optical Transport Network. *J. Light. Technol.* **2010**, *24*, 4711–4728. [CrossRef]
18. Adams, R.; Spasojevic, M.; Chagnon, M.; Malekiha, M.; Li, J.; Plant, D.V.; Chen, L.R. Wavelength conversion of 28 GBaud 16-QAM signals based on four-wave mixing in a silicon nanowire. *Opt. Express* **2014**, *22*, 4083–4090. [CrossRef] [PubMed]
19. Da Ros, F.; Vukovic, D.; Gajda, A.; Dalgaard, K.; Zimmermann, L.; Tillack, B.; Galili, M.; Petermann, K.; Peucheret, C. Phase regeneration of DPSK signals in a silicon waveguide with reverse-biased p-i-n junction. *Opt. Express* **2014**, *22*, 5029–5036. [CrossRef] [PubMed]

20. Dolgaleva, K.; Ng, W.; Qian, L.; Aitchison, J. Compact highly-nonlinear AlGaAs waveguides for efficient wavelength conversion. *Opt. Express* **2011**, *19*, 1496–1498. [CrossRef] [PubMed]
21. Lacava, C.; Pusino, V.; Minzioni, P.; Sorel, M.; Cristiani, I. Nonlinear properties of AlGaAs waveguides in continuous wave operation regime. *Opt. Express* **2014**, *22*, 5291–5298. [CrossRef] [PubMed]
22. Eggleton, B.J.; Luther-Davies, B.; Richardson, K. Chalcogenide photonics. *Nat. Photonics* **2011**, *5*, 141–148.
23. Ahmad, R.; Rochette, M. High efficiency and ultra broadband optical parametric four-wave mixing in chalcogenide-PMMA hybrid microwires. *Opt. Express* **2012**, *20*, 9572–9580. [CrossRef] [PubMed]
24. Moss, D.J.; Morandotti, R.; Gaeta, A.L.; Lipson, M. New CMOS-compatible platforms based on silicon nitride and Hydex for nonlinear optics. *Nat. Photonics* **2013**, *7*, 597–607. [CrossRef]
25. Koos, C.; Vorreau, P.; Vallaitis, T.; Dumon, P. All-optical high-speed signal processing with silicon – organic hybrid slot waveguides. *Nat. Photonics* **2009**, *3*, 1–4. [CrossRef]
26. Lacava, C.; Ettabib, M.; Cristiani, I.; Fedeli, J.; Richardson, D.; Petropoulos, P. Ultra-Compact Amorphous Silicon Waveguide for Wavelength Conversion. *IEEE Photonics Technol. Lett.* **2016**, *28*, 410–414. [CrossRef]
27. Ettabib, M.A.; Kapsalis, A.; Bogris, A.; Parmigiani, F.; Rancano, V.J.F.; Bottrill, K.; Brun, M.; Labeye, P.; Nicoletti, S.; Hammani, K.; et al. Polarization Insensitive Wavelength Conversion in a Low-Birefringence SiGe Waveguide. *IEEE Photonics Technol. Lett.* **2016**, *28*, 1221–1224. [CrossRef]
28. Lacava, C.; Minzioni, P.; Baldini, E.; Tartara, L.; Fedeli, J.M.; Cristiani, I. Nonlinear characterization of hydrogenated amorphous silicon waveguides and analysis of carrier dynamics. *Appl. Phys. Lett.* **2013**, *103*. [CrossRef]
29. Ettabib, M.A.; Parmigiani, F.; Kapsalis, A.; Bogris, A.; Brun, M.; Labeye, P.; Nicoletti, S.; Hammani, K. Record Phase Sensitive Extinction Ratio in a Silicon Germanium Waveguide. In Proceedings of the Lasers and Electro-Optics (CLEO 2015), San Jose, CA, USA, 10–15 May 2015.
30. Ettabib, M.A.; Bottrill, K.; Parmigiani, F.; Kapsalis, A.; Bogris, A.; Brun, M.; Labeye, P.; Nicoletti, S.; Hammani, K.; Syvridis, D. All-optical Phase Regeneration with Record PSA Extinction Ratio in a Low-birefringence Silicon Germanium Waveguide. *J. Light. Technol.* **2016**, *34*, 3993–3998. [CrossRef]
31. Ettabib, M.A.; Xu, L.; Bogris, A.; Kapsalis, A.; Belal, M.; Lorent, E.; Labeye, P.; Nicoletti, S.; Hammani, K.; Syvridis, D.; et al. Broadband telecom to mid-infrared supercontinuum generation in a dispersion-engineered silicon germanium waveguide. *Opt. Lett.* **2015**, *40*, 4118–4121. [CrossRef] [PubMed]
32. Grillet, C.; Carletti, L.; Monat, C.; Grosse, P.; Ben Bakir, B.; Menezo, S.; Fedeli, J.M.; Moss, D.J. Amorphous silicon nanowires combining high nonlinearity, FOM and optical stability. *Opt. Express* **2012**, *20*, 22609–22615. [CrossRef] [PubMed]
33. Suda, S.; Tanizawa, K.; Sakakibara, Y.; Kamei, T.; Nakanishi, K.; Itoga, E.; Ogasawara, T.; Takei, R.; Kawashima, H.; Namiki, S.; et al. Pattern-effect-free all-optical wavelength conversion using a hydrogenated amorphous silicon waveguide with ultra-fast carrier decay. *Opt. Lett.* **2012**, *37*, 1382–1384. [CrossRef] [PubMed]
34. Narayanan, K.; Elshaari, A.W.; Preble, S.F. Broadband all-optical modulation in hydrogenated-amorphous silicon waveguides. *Opt. Express* **2010**, *18*, 9809–9814. [CrossRef] [PubMed]
35. Matres, J.; Ballesteros, G.C.; Gautier, P.; Fédéli, J.-M.; Martí, J.; Oton, C.J. High nonlinear figure-of-merit amorphous silicon waveguides. *Opt. Express* **2013**, *21*, 3932–3940. [CrossRef] [PubMed]
36. Kuyken, B.; Clemmen, S.; Selvaraja, S.K.; Bogaerts, W.; Van Thourhout, D.; Emplit, P.; Massar, S.; Roelkens, G.; Baets, R. On-chip parametric amplification with 26.5 dB gain at telecommunication wavelengths using CMOS-compatible hydrogenated amorphous silicon waveguides. *Opt. Lett.* **2011**, *36*, 552–554. [CrossRef] [PubMed]
37. Mehta, P.; Healy, N.; Day, T.D.; Badding, J.V.; Peacock, A.C. Ultrafast wavelength conversion via cross-phase modulation in hydrogenated amorphous silicon optical fibers. *Opt. Express* **2012**, *20*, 26110–26116. [CrossRef] [PubMed]
38. Kuyken, B.; Ji, H.; Clemmen, S.; Selvaraja, S.K.; Hu, H.; Pu, M.; Galili, M.; Jeppesen, P.; Morthier, G.; Massar, S.; et al. Nonlinear properties of and nonlinear processing in hydrogenated amorphous silicon waveguides. *Opt. Express* **2011**, *19*, B146–B153. [CrossRef] [PubMed]
39. Taillaert, D.; Bienstman, P.; Baets, R. Compact efficient broadband grating coupler for silicon-on-insulator waveguides. *Opt. Lett.* **2004**, *29*, 2749–2751. [CrossRef] [PubMed]
40. Agrawal, G.P. *Nonlinear Fiber Optics*, 5th ed.; Elsevier, Ed.; Academic Press: New York, NY, USA, 2013.

41. Tsang, H.K.; Liu, Y. Nonlinear optical properties of silicon waveguides. *Semicond. Sci. Technol.* **2008**, *23*. [CrossRef]
42. Lin, Q.; Painter, O.J.; Agrawal, G.P. Nonlinear optical phenomena in silicon waveguides: Modeling and applications. *Opt. Express* **2007**, *15*, 16604–16644. [CrossRef] [PubMed]
43. Wang, K.-Y.; Foster, A.C. Ultralow power continuous-wave frequency conversion in hydrogenated amorphous silicon waveguides. *Opt. Lett.* **2012**, *37*, 1331–1333. [CrossRef] [PubMed]
44. Shen, L.; Healy, N.; Mehta, P.; Day, T.D.; Sparks, J.R.; Badding, J.V.; Peacock, A.C. Nonlinear transmission properties of hydrogenated amorphous silicon core fibers towards the mid-infrared regime. *Opt. Express* **2013**, *21*, 13075–13083. [CrossRef] [PubMed]
45. Narayanan, K.; Preble, S.F. Optical nonlinearities in hydrogenated-amorphous silicon waveguides. *Opt. Express* **2010**, *18*, 8998–9005. [CrossRef] [PubMed]
46. Chagnon, M.; Spasojevic, M.; Adams, R.; Li, J.; Plant, D.V.; Chen, L.R. Wavelength Multicasting at 22-GBaud 16-QAM in a Silicon Nanowire Using Four-Wave Mixing. *IEEE Photonics Technol. Lett.* **2015**, *27*, 860–863. [CrossRef]
47. Ros, F.D.; Yankov, M.P.; Silva, E.P.; Pu, M.; Ottaviano, L.; Hu, H. Characterization of a Wavelength Converter for 256-QAM Signals Based on an AlGaAs-On-Insulator. *Nano-Waveguide* **2016**, *1*, 662–664.
48. Filion, B.; Ng, W.C.; Nguyen, A.T.; Rusch, L.A.; Larochelle, S. Wideband wavelength conversion of 16 Gbaud 16-QAM and 5 Gbaud 64-QAM signals in a semiconductor optical amplifier. *Opt. Express* **2013**, *21*, 19825–19833. [CrossRef] [PubMed]
49. Paul, D.J. Si/SiGe heterostructures: From material and physics to devices and circuits. *Semicond. Sci. Technol.* **2004**, *19*, R75–R108. [CrossRef]
50. Roth, J.E.; Fidaner, O.; Schaevitz, R.K.; Kuo, Y.-H.; Kamins, T.I.; Harris, J.S.; Miller, D.A.B. Optical modulator on silicon employing germanium quantum wells. *Opt. Express* **2007**, *15*, 5851–5859. [CrossRef] [PubMed]
51. Tsybeskov, L.; Lockwood, D.J. Silicon-germanium nanostructures for light emitters and on-chip optical interconnects. *Proc. IEEE* **2009**, *97*, 1284–1303. [CrossRef]
52. Chen, L.; Lipson, M. Ultra-low capacitance and high speed germanium photodetectors on silicon. *Opt. Express* **2009**, *17*, 7901–7906. [CrossRef] [PubMed]
53. Vivien, L.; Polzer, A.; Marris-Morini, D.; Osmond, J.; Hartmann, J.M.; Crozat, P.; Cassan, E.; Kopp, C.; Zimmermann, H.; Fédéli, J.M. Zero-bias 40 Gbit/s germanium waveguide photodetector on silicon. *Opt. Express* **2012**, *20*, 1096–1101. [CrossRef] [PubMed]
54. Ettabib, M.A.; Hammani, K.; Parmigiani, F.; Jones, L.; Kapsalis, A.; Bogris, A.; Syvridis, D.; Brun, M.; Labeye, P.; Nicoletti, S.; et al. FWM-based wavelength conversion of 40 Gbaud PSK signals in a silicon germanium waveguide. *Opt. Express* **2013**, *21*, 17–23. [CrossRef] [PubMed]
55. Hammani, K.; Ettabib, M.A.; Bogris, A.; Kapsalis, A.; Syvridis, D.; Brun, M.; Labeye, P.; Nicoletti, S.; Richardson, D.J.; Petropoulos, P. Optical properties of silicon germanium waveguides at telecommunication wavelengths. *Opt. Express* **2013**, *21*, 16690–16701. [CrossRef] [PubMed]
56. Tittelbach, G.; Richter, B.; Karthe, W. Comparison of three transmission methods for integrated optical waveguide propagation loss measurement. *Pure Appl. Opt.* **1993**, *2*, 683–706. [CrossRef]
57. Ettabib, M.; Lacava, C.; Liu, Z.; Bogris, A.; Kapsalis, A.; Brun, M.; Labeye, P.; Nicoletti, S.; Syvridis, D.; Richardson, D.J.; et al. Wavelength Conversion of 16-QAM and 64-QAM Signals in a Compact SiGe Waveguide. *Manuscr. Submitt. Publ.* **2016**, in press.
58. Ros, F.D.; Porto, E.; Zibar, D.; Chu, S.T.; Little, B.E.; Morandotti, R.; Galili, M.; Moss, D.J.; Oxenløwe, L.K. Low-penalty up to 16-QAM wavelength conversion in a low loss CMOS compatible spiral waveguide. In Proceedings of the Optical Fiber Communication Conference, Anaheim, CA, USA, 20–24 March 2016.
59. Xing, L.; Pu, M.; Zhou, B.; Clemens, K.; Attila, F.; Torres-Company, V.; Bache, M. Octave-spanning supercontinuum generation in a silicon-rich nitride waveguide. *Opt. Lett.* **2016**, *41*, 2719–2722.
60. Krückel, C.J.; Torres-Company, V.; Andrekson, P.A.; Spencer, D.T.; Bauters, J.F.; Heck, M.J.R.; Bowers, J.E. Continuous wave-pumped wavelength conversion in low-loss silicon nitride waveguides. *Opt. Lett.* **2015**, *40*, 875–878. [CrossRef] [PubMed]
61. Baets, R.; Subramanian, A.Z.; Clemmen, S.; Kuyken, B.; Bienstman, P.; Nicolas, T.L.; Roelkens, G.; Van Thourhout, D.; Hein, P.; Severi, S. Silicon Photonics: Silicon nitride versus silicon-on-insulator. In Proceedings of the Optical Fiber Communication Conference, Anaheim, CA, USA, 20–24 March 2016.

62. Bauters, J.F.; Heck, M.J.R.; John, D.; Dai, D.; Tien, M.-C.; Barton, J.S.; Leinse, A.; Heideman, R.G.; Blumenthal, D.J.; Bowers, J.E. Ultra-low-loss high-aspect-ratio Si_3N_4 waveguides. *Opt. Express* **2011**, *19*, 3163–3174. [CrossRef] [PubMed]
63. Levy, J.; Foster, M.; Gaeta, A.L.; Lipson, M. Harmonic generation in silicon nitride ring resonators. *Opt. Express* **2011**, *19*, 11415–11421. [CrossRef] [PubMed]
64. Tien, M.-C.; Bauters, J.F.; Heck, M.J.R.; Blumenthal, D.J.; Bowers, J.E. Ultra-low loss Si_3N_4 waveguides with low nonlinearity and high power handling capability. *Opt. Express* **2010**, *18*, 23562–23568. [CrossRef] [PubMed]
65. Choi, J.W.; Chen, G.F.R.; Ng, D.K.T.; Ooi, K.J.A.; Tan, D.T.H. Wideband nonlinear spectral broadening in ultra-short ultra—silicon rich nitride waveguides. *Sci. Rep.* **2016**, 1–8. [CrossRef] [PubMed]
66. Krückel, C.J.; Fülöp, A.; Klintberg, T.; Bengtsson, J.; Andrekson, P.A.; Torres-Company, V. Linear and nonlinear characterization of low-stress high-confinement silicon-rich nitride waveguides. *Opt. Express* **2015**, *23*, 25827–25837. [CrossRef] [PubMed]
67. Wang, T.; Ng, D.K.T.; Ng, S.; Toh, Y.; Chee, A.K.L.; Chen, G.F.R.; Wang, Q.; Tan, D.T.H. Supercontinuum generation in bandgap engineered, back-end CMOS compatible silicon rich nitride waveguides. *Laser Photonics Rev.* **2015**, *9*, 498–506. [CrossRef]
68. Lacava, C.; Stankovic, S.; Khokhar, A.Z.; Bucio, T.D.; Gardes, F.Y.; Richardson, D.J.; Reed, G.T. CMOS-compatible Silicon-Rich Nitride Waveguides for Ultrafast Nonlinear Signal Processing. In Proceedings of the Conference on Lasers and Electro-Optics, San Jose, CA, USA, 5–10 June 2016.
69. Lacava, C.; Stankovic, S.; Khokhar, A.Z.; Bucio, T.D.; Gardes, F.; Reed, G.T.; Richardson, D.J.; Petropoulos, P. Si-rich Silicon Nitride for Nonlinear Signal Processing Applications. *Sci. Rep. Nat. Publ. Group* **2016**, in press.
70. Tai, C.-Y.; Wilkinson, J.S.; Perney, N.M.B.; Netti, M.C.; Cattaneo, F.; Finlayson, C.E.; Baumberg, J.J. Determination of nonlinear refractive index in a Ta_2O_5 rib waveguide using self-phase modulation. *Opt. Express* **2004**, *12*, 5110–5116. [CrossRef] [PubMed]
71. Lacava, C.; Aghajani, A.; Hua, P.; Richardson, D.J.; Petropoulos, P.; Wilkinson, J.S. Nonlinear optical properties of ytterbium-doped tantalum pentoxide rib waveguides on silicon at telecom wavelengths. In Proceedings of the Optical Fiber Communication Conference, Anaheim, CA, USA, 20–24 March 2016.
72. Wu, C.-L.; Chiu, Y.-J.; Chen, C.-L.; Lin, Y.-Y.; Chu, A.-K.; Lee, C.-K. Four-wave-mixing in the loss low submicrometer Ta_2O_5 channel waveguide. *Opt. Lett.* **2015**, *40*, 4528–4531. [CrossRef] [PubMed]
73. Aghajani, A.; Murugan, G.S.; Sessions, N.P.; Apostolopoulos, V.; Wilkinson, J.S. Waveguide lasers in ytterbium-doped tantalum pentoxide on silicon. *Opt. Lett.* **2015**, *40*, 2549–2552. [CrossRef] [PubMed]